

# Space Weather



## RESEARCH ARTICLE

10.1029/2020SW002704

### Key Points:

- Geosynchronous magnetopause crossings are studied in connection with solar wind drivers and accompanying geomagnetic activity
- Dst index often reaches a minimum in 3–8 h after geosynchronous magnetopause crossings
- Average SML (SMU) index reach minimum (maximum) in one hour after geosynchronous magnetopause crossings

### Supporting Information:

Supporting Information may be found in the online version of this article.

### Correspondence to:

A. A. Samsonov,  
[a.samsonov@ucl.ac.uk](mailto:a.samsonov@ucl.ac.uk)

### Citation:








Samsonov, A. A., Bogdanova, Y. V., Branduardi-Raymont, G., Xu, L., Zhang, J., Sormakov, D., et al. (2021). Geosynchronous magnetopause crossings and their relationships with magnetic storms and substorms. *Space Weather*, 19, e2020SW002704. <https://doi.org/10.1029/2020SW002704>

Received 16 DEC 2020  
 Accepted 26 MAY 2021

© 2021. The Authors.

This is an open access article under the terms of the [Creative Commons Attribution](https://creativecommons.org/licenses/by/4.0/) License, which permits use, distribution and reproduction in any medium, provided the original work is properly cited.

## Geosynchronous Magnetopause Crossings and Their Relationships With Magnetic Storms and Substorms

A. A. Samsonov<sup>1</sup> , Y. V. Bogdanova<sup>2</sup> , G. Branduardi-Raymont<sup>1</sup> , L. Xu<sup>1</sup>, J. Zhang<sup>1</sup> , D. Sormakov<sup>3</sup> , O. A. Troshichev<sup>3</sup> , and C. Forsyth<sup>1</sup> 

<sup>1</sup>Mullard Space Science Laboratory, University College London, Dorking, Surrey, UK, <sup>2</sup>RAL Space, Rutherford Appleton Laboratory, Science and Technology Facilities Council, Didcot, Oxfordshire, UK, <sup>3</sup>Arctic and Antarctic Research Institute, St. Petersburg, Russia

**Abstract** The paper investigates the strengthening of magnetospheric activity related to geosynchronous magnetopause crossings (GMCs). We make a list of GMC events using the empirical magnetopause model (Lin et al., 2010, <https://doi.org/10.1029/2009ja014235>) and hourly averaged OMNI data and find which solar wind and magnetospheric conditions accompany and follow the GMCs. The GMCs are mostly caused by the impact of interplanetary coronal mass ejections (ICMEs) and/or interplanetary shocks often with a strong increase in the density and a moderate increase in velocity. The average solar wind density during the first GMC hour is higher than  $20 \text{ cm}^{-3}$  in 70% cases, while the velocity is higher than 500 km/s in 56% cases. The hourly interplanetary magnetic field (IMF)  $B_Z$  is negative in 87% cases. The average over all events SMU (SML), Kp, and PC indices reach maxima (minima) in 1 h after the GMC beginning, while the delay of the minimum of the Dst index is usually 3–8 h. These average time delays do not depend on the strength of the storms and substorms. The SML (Dst) minimum is less than  $-500 \text{ nT}$  ( $-30 \text{ nT}$ ) in the next 24 h in 95% (99%) cases, that is, the GMC events are mostly followed by magnetic storms and substorms. We compare solar wind and magnetospheric conditions for GMCs connected with ICMEs and stream interaction regions (SIRs). Our study confirms that the ICME-related events are characterized by stronger ring current and auroral activity than the SIR-related events. The difference might be explained by the different behavior of the solar wind velocity.

**Plain Language Summary** With an ever-increasing number of satellites in geostationary orbit, it is crucial to predict when they will be located outside of the Earth's magnetosphere which shields satellites from the interplanetary medium, including the low-energy part of the solar energetic particle spectra which can potentially damage exposed satellite systems. Here, using a well-established empirical model, we show that such satellites are outside of the protective magnetic shield in rare cases of extreme magnetospheric compression, as only 100 cases were identified over 24 years. We demonstrate that most of the cases occur during the times when the Sun is most active and are associated with Interplanetary Coronal Mass Ejections, giant bubbles of plasma occasionally emitted from the Sun and propagating through space. The disturbances of the near-Earth space associated with the times of extreme magnetospheric compression are analyzed. It is shown that such compressions are followed by local geomagnetic activity at the high-latitudes in the nightside (“magnetospheric substorm”) with an average time delay of 1 h and by global magnetic disturbances (“magnetic storm”) with the maximum effect observed by 3–8 h later.

## 1. Introduction

Interplanetary coronal mass ejections (ICMEs) and stream interaction regions (SIRs) (some of them also referred as corotating interaction regions (CIRs) (Jian et al., 2006)) reaching the Earth's magnetosphere initiate disturbances in different magnetospheric regions, lead to intensifications of the magnetospheric-ionospheric (MI) currents, and generally increase the magnetospheric activity. A most powerful form of the magnetospheric activity is magnetic storms with intensification of the ring current and magnetic field variations over the globe. Another significant form is substorms characterized by intensification of the nightside MI currents and injection of energetic particles from the magnetotail into the inner magnetosphere and auroral regions. Both magnetic storms and substorms are typically identified by indices of magnetospheric activity. However, they are not the only signatures of high magnetospheric activity. An increase

in the magnetospheric activity in response to ICMEs and CIRs often begins with a strong magnetospheric compression. In particular, the dayside magnetopause may pass a geostationary orbit also referred to as a geosynchronous equatorial orbit (GEO), thereby geostationary spacecraft near noon would observe geosynchronous magnetopause crossings (GMCs). Many communication, navigation, and weather satellites are located on GEO, and the passing through magnetosheath or solar wind may damage the satellite equipment and/or impact the spacecraft operations.

Since the nineteenth century, many global magnetic disturbances (magnetic storms) have been observed to begin with a sudden commencement (e.g., Adams, 1892), that is, an abrupt increase in the ground horizontal magnetic field quantified by the Dst index. Later, it became clear that the sudden commencements result from impact of interplanetary (IP) shocks (or sometimes of tangential discontinuities) which compress the magnetosphere (Sonett et al., 1964). However, some magnetic storms (e.g., many of those related to CIRs (Borovsky & Denton, 2006)) are not preceded by sudden commencements, while solar wind dynamic pressure jumps associated with either IP shocks or tangential discontinuities do not necessarily result in magnetic storms (Joselyn & Tsurutani, 1990; Smith et al., 2020, and references therein). Similarly, some magnetospheric substorms have been found to be triggered externally by sudden increase in the solar wind dynamic pressure (e.g., Burch, 1972; Keika et al., 2009; Kokubun et al., 1977; Zhou & Tsurutani, 2001;), while some authors (e.g., Aubry & McPherron, 1971; Liou et al., 2003; Rostoker, 1983; McPherron et al., 1986;) conclude that northward interplanetary magnetic field (IMF) turning is a most significant triggering mechanism. Furthermore, some substorms have no clear solar wind drivers and are supposed to be driven by internal instabilities in the plasma sheet (Henderson et al., 1996; Horwitz, 1985; McPherron et al., 1986). Preconditioning has been noted as having an important role in triggering of both substorms (e.g., Lyons et al., 2005; Morley & Freeman, 2007) and magnetic storms (e.g., Echer et al., 2011; Gosling et al., 1991; Tsurutani et al., 1988). For instance, intervals of strong negative IMF  $B_z$  (e.g., several hours of  $B_z < -10$  nT) before a solar wind trigger (e.g., an interplanetary shock) greatly increase the geoeffectiveness of the trigger and result in strong magnetic storms or substorms. Troshichev and Sormakov (2019a) compared the response of the auroral AL index to solar wind pressure pulses separately for northward and southward IMFs and found that the average AL index significantly changes only for conditions with a steady southward IMF. In general, the solar wind energy input into the magnetosphere is controlled by the solar wind velocity and IMF magnitude and clock angle. These solar wind parameters and their combinations show a good correlation with the indices of magnetospheric activity (e.g., Newell et al., 2007, and referenes therein).

Magnetic storms and substorms have been a subject of active studies for many tens of years, while GMCs have not attracted such a great attention by the scientific community so far. This may be partly related to some difficulties with observations of GMCs. Among a large number of GEO satellites, only some of them carry scientific instruments and measure whether the magnetic field or energetic particles. While magnetic storms and substorms are easily identified by continuous time series of magnetospheric indices available for tens of years, we can use only scattered GMC observations obtained by GEO spacecraft. Recently, it has been noticed that extreme magnetospheric compression plays a significant role in draining electrons from the outer radiation belt due to the magnetopause shadowing effect (Olifer et al., 2019; Staples et al., 2020; Tu et al., 2019; Turner et al., 2012).

Although in-situ observations are scattered, there is another way to make a continuous GMC database with the help of empirical magnetopause models. Empirical magnetopause models (e.g., Dmitriev & Suvorova, 2000; Lin et al., 2010; Petrinc & Russell, 1996; Sibeck et al., 1991; Shue et al., 1998; Wang et al., 2013) are based on a large data set of the available magnetopause crossings (not only GMCs) and usually (except Dmitriev & Suvorova, 2000; Wang et al., 2013) apply some analytical expressions to describe the magnetopause shape in dependence on the solar wind conditions and sometimes on the dipole tilt. In particular, the Shue et al. (1998)'s model presented an axisymmetric magnetopause with the magnetopause stand-off distance and flaring angle depending on the solar wind dynamic pressure and the IMF  $B_z$ . Later, the Lin et al. (2010)'s model used a larger data set and suggested a 3-D magnetopause shape whose coefficients depend on the solar wind dynamic and magnetic pressure, IMF  $B_z$ , and also the dipole tilt. Dmitriev et al. (2016) compared the ability of several magnetopause models in prediction of GMCs and concluded that the model of Lin et al. (2010) demonstrated the best capability of GMC prediction in a wide range of geomagnetic disturbances from severe to extremely strong magnetic storms. We believe that GMCs will attract

more attention and be better predicted in the future, especially when new missions, like the Solar Wind Magnetosphere Ionosphere Link Explorer (SMILE) (Raab et al., 2016), will be launched. Using SMILE, we will be able to obtain a continuous time series of the magnetopause standoff distance for variable solar wind conditions and also validate prospective empirical models. In addition, the continuous SMILE observations of magnetospheric compressions and expansions can indicate the times of arrival of solar wind structures (e.g., ICMEs, CIRs) which would change the global state of the magnetosphere and its activity.

Any impact of a solar wind pressure pulse on the magnetosphere results in two effects. The first is general magnetospheric compression usually accompanied by increase in the magnetopause electric current observed as a sudden impulse (sudden commencement) on the ground. The second is increase in the energy transfer rate from the solar wind into the magnetosphere which becomes significant for a southward IMF due to the magnetopause reconnection (see, e.g., Newell et al., 2007; Samsonov et al., 2020). The time scale of the first process is only several minutes, while the second process may result in increase of the global magnetospheric activity, lead to substorms and magnetic storms, and respectively has a longer time scale measured by hours. With potential space weather applications of the SMILE observations in mind, the purpose of this work is to study the increase in the magnetospheric activity accompanying and following GMCs, in particular looking at variations of the magnetospheric indices which characterize magnetic storms and substorms. Therefore, we will consider mostly the second effect of the increase in the dynamic pressure. We find the time delays between the GMC events and following minima of the Dst and SML indices and maxima of the SMU index. Note that SML and SMU are the two SuperMAG indices which characterize the auroral electrojet and are calculated in a similar way to the traditional *AL* and *AU* indices, but use observations from a larger number of magnetometers (100 or more stations instead of 12 used for the *AL* and *AU*). Respectively, the SuperMAG indices are able to reveal some substorms which may be missed by using the traditional auroral indices (Newell & Gjerloev, 2011). The SML index, similarly to the *AL* index, is supposed to represent the substorm activity, while the SMU index is a measure of the eastward electrojet possibly related to the dayside reconnection. Note also that the SME index is defined as the difference between SMU and SML (for more details see Newell & Gjerloev, 2011).

We determine the range of solar wind parameters for which the GMC events occur. In order to do this we use the empirical Lin et al. (2010)'s magnetopause model to make a list of GMC events. We realize that the model may occasionally underestimate or overestimate the magnetopause standoff distance and, correspondingly, some GMC events may be missed and some other events may be erroneously included in the list. However, despite a possible inaccuracy in several cases the Lin et al. (2010)'s model generally well reproduces the magnetopause compressions and expansions and applies to GMC events better than other models (Dmitriev et al., 2016).

This paper is structured as follows. In the next section, we describe the method of selection of GMC events. The third section discusses how the number of GMCs varies with solar activity. The next section presents one example consisting of three successive GMCs and displays the magnetospheric response in this event. The fifth section analyzes the solar wind conditions for the GMC events, while the sixth section discusses the magnetospheric conditions expressed by the SML and SMU (Gjerloev, 2012; Newell & Gjerloev, 2011), Dst (Nose et al., 2015), PC (Troshichev & Andrezen, 1985; Troshichev et al., 1988) (often referred to as a proxy of the solar wind energy that entered into the magnetosphere (Troshichev et al., 2014)) and *Kp* (Bartels, 1949) indices. In the seventh section, we compare solar wind and magnetospheric conditions for GMC events connected with ICMEs and SIR/CIRs, and the last section concludes the paper. In Supporting Information, we provide a list of our events and classify them as connected to either ICMEs or SIR/CIRs and to IP shocks if possible.

## 2. Selection of GMC Events

In this study, we use the hourly average solar wind parameters from OMNI (<https://omniweb.gsfc.nasa.gov/>) and consider the time interval from 1995 to 2018 because the solar wind OMNI data before 1995 contain many data gaps (Samsonov et al., 2019). Recent studies based on 1 min data (Troshichev & Sor-makov, 2019b; Vokhmyanin et al., 2019) showed that sometimes there is a discrepancy between the OMNI data set and observations in front of the bow shock. We believe, however, that the correlation between data

at L1 (used for the OMNI) and at the bow shock becomes better if using 1 h resolution data since only the variations on a large spatial scale are correlated in this case. We calculate the magnetopause standoff distance using the Lin et al. (2010)'s model (L10 model below). In this model, the standoff distance depends on the solar wind parameters (dynamic and magnetic pressures, and IMF  $B_z$ ) and slightly depends on the dipole tilt. However, we neglect the tilt dependence because our primary purpose is to select time intervals with strong magnetospheric compression caused by variations of the solar wind parameters. In general, the difference between the standoff distance for tilted and nontilted dipoles at the subsolar point is insignificant (Samsonov et al., 2016).

We search the “first GMC events,” that is, the first time when the standoff distance  $R_{SUB} < 6.62 R_E$ . Then we skip 24 h after the “first” GMC and define this interval as one event. As we will show below, most GMCs result from ICME impact on the magnetosphere. The empirical model often predicts multiple magnetopause crossings during the next 24 h after a first GMC, therefore it seems reasonable to combine several crossings in one event for our study. Applying this method for the years 1995–2018, we obtain a list of 100 “first” GMCs. We exclude the event on November 5, 2001 from the list because of multiple data gaps in the solar wind data, finally forming a list of 99 events. We provide this list in the Supporting Information. If we prolong the time interval after “first” GMCs up to 48 h, three cases will be absorbed by previous GMCs and the list of “first” GMCs will contain 96 events (again after excluding the same event with data gaps). During this study, we drew a set of plots for the 48 h intervals like those we present below for 24 h. Since the results obtained for the 48 h intervals confirm our conclusions made for the 24 h intervals, we do not include them in the paper to avoid repetitions.

In order to characterize external sources of the strong magnetospheric compression, we have compared our list of GMC events with the published catalogs of the ICMEs and SIR/CIRs. The Richardson and Cane ICME catalog (Cane & Richardson, 2003; Richardson & Cane, 2010), available at: <http://www.srl.caltech.edu/ACE/ASC/DATA/level3/icmetable2.htm> and covering January 1996–February 2021, was used for the related ICME search. For the CIR/SIR search, three different catalogs have been used: (a) the catalog published in Jian et al. (2006), covering the period of 1995–2004; (b) the catalog published in Zhang et al. (2007), covering the period of 1996–2005; and (c) the catalog developed based on the STEREO CIR/SIR observations, available at [https://www.helcats-fp7.eu/catalogues/wp5\\_cat.html](https://www.helcats-fp7.eu/catalogues/wp5_cat.html), covering 2007–2015. The last catalog has been used with caution due to STEREO being far from the Sun–Earth line during 2010–2015. For the GMC events not associated with the ICMEs and not covered by the CIR/SIR catalogs we have examined the solar wind and IMF parameters, based on the OMNI data (<https://omniweb.gsfc.nasa.gov/>) to check for the CIR/SIR signatures. The SIR identification was based on the criteria outlined in Jian et al. (2006); Richardson (2018): (a) increase in the solar wind velocity, (b) observation of the total pressure peak during the velocity increase, with a slow increase/decrease on both sides of the peak, (c) compression of the density and magnetic field at the interface between slow and fast solar wind, as well as the temperature increase. The results of the external sources identification are presented in the Table S1 in the Supporting Information. Here, the times for ICMEs correspond to the time of associated geomagnetic storm sudden commencement (typically related to the arrival of an IP shock at Earth). Otherwise, “A” indicates the time of shock passage at ACE, “W” indicates the time of a shock at the WIND spacecraft if not also reported at ACE. The dates for CIRs from Zhang et al. (2007) catalog correspond to the minima of the Dst index and from Jian et al. (2006) catalog — to the stream interface observed at Wind or ACE. Since the ICME and SIR catalogs may not include all strong solar wind disturbances, in addition we have used the published catalogs of IP shocks mentioned below. Oliveira and Raeder (2015) collected a list of IP shocks using both ACE and WIND data from 1995 to 2013. We have also used the shock database from the Harvard-Smithsonian Center for astrophysics at <https://www.cfa.harvard.edu/shocks/>.

We classify 74 events (i.e., 75%) as ICMEs and 18 events (18%) as SIR/CIRs; 76 GMC events follow IP shocks. Thus only seven GMC crossings are connected neither to the ICMEs nor SIR/CIRs according to the above-mentioned catalogs and our analysis, although they still occur during disturbed solar wind conditions with significant increases in the velocity and density. If we combine together all the solar wind structures (ICMEs, SIRs, and IP shocks) which cause strong magnetospheric compressions, we will find that all the GMCs in our list are connected with at least one of the solar wind sources mentioned in the catalogs or identified by ourself (only SIR/CIRs).



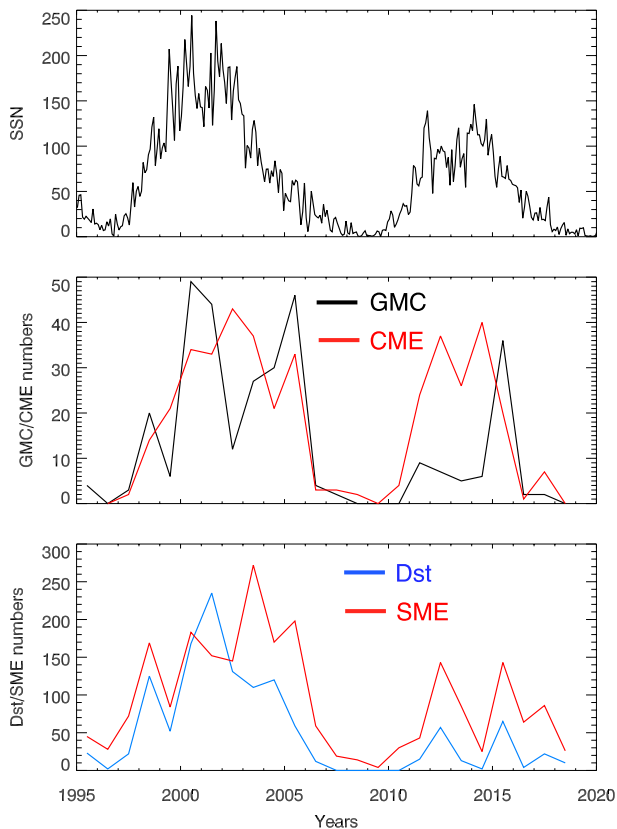


**Figure 1.** Top: monthly average total sunspot number (SSN). Middle: total number of geosynchronous magnetopause crossing (GMC) hours (black) and number of CMEs with the speed higher than 900 km/s and the angular width higher than  $100^\circ$  from the SOHO LASKO catalog (red). Bottom: number of hours with Dst <  $-100$  nT (blue) and number of hours with SME > 1,000 nT (red).

We note that for the majority of the events the time lag between the ICMEs and GMCs varies from tens of minutes to a few hours indicating a clear connection between the solar wind structures and magnetospheric compression. Occasionally the observed time difference was rather large, reaching more than 24 h in five events. We suggest that long time delays may correspond to more complex solar wind conditions, for example, two interacting ICMEs (or an ICME and a SIR/CIR), with the first of them being identified in the ICME catalog, and the second resulting in the GMC event. There were also several events with GMCs observed slightly earlier than ICMEs. For example, on November 7 and 9, 2004, the two ICMEs from the catalog occur after the two corresponding GMC events, however, two IP shocks were observed by ACE several hours before the GMCs. Again, this complex behavior might be explained by the interaction of two ICMEs, with the first ICME causing the GMC and the second being included in the catalog. Table S1 in the Supporting Information also indicates the events with a duration longer than 1 h (i.e., when the hourly average standoff distance keeps less than  $6.62 R_E$  for several hours). We find 63 such events (64%).

We compare predictions of the L10 model with spacecraft observations at geosynchronous orbit. Geosynchronous spacecraft observe GMCs only in the dayside region. We think that the basic undoubted evidence of GMC event is a trace of negative  $B_z$  in magnetic field data. We have checked predictions of the empirical model using GOES observations for one year, 2005. This year is characterized by a relatively high solar activity, therefore we identify 13 GMC events in 2005. We use GOES 10 and GOES 12 magnetic field data for validation of the empirical model. In 4 of 13 events, GOES observed clear GMCs (with  $B_z < 0$ ) in the dayside region. Among the remaining nine events, we search only the events with one GOES in the subsolar region, from 9 to 15 MLT. We find only one such event (12.06.2005) when GOES 12 was located about 13 MLT at 18 UT (the time of predicted GMC). We inspect this event more carefully and find a brief trace of negative  $B_z$  at 17:27 UT observed by

GOES 12. In this event, an ICME with a strong negative IMF  $B_z$  interacts with the magnetosphere and solar wind parameters slowly vary during several hours. The model predicts only one hour of  $R_{SUB} < 6.62 R_E$  at 18 UT. This is nearly the same of what GOES observations show since we observe a brief GMC slightly before 18 UT in this case. Therefore we conclude that predictions of the empirical model agree well with GOES data in 2005.

### 3. Solar Cycle Variations

The average magnetopause standoff distance varies with solar activity (Samsonov et al., 2019). Nemecek et al. (2016) discussed the contribution of other parameters, besides the solar wind dynamic pressure and IMF  $B_z$ , in the variations of the magnetopause location in the two last solar cycles. Figure 1 collects the monthly average sunspot number (SSN), the total number of GMC hours and the number of ICMEs with high speed and large angular width, and the total length of time of extreme Dst and SME indices from 1995 to 2018 (see figure caption for more detail). Note that we calculate the total intervals of GMC (not only “first” GMCs) and extreme indices in hours for this figure to compare one with the other. The time interval covers the 23<sup>rd</sup> and 24<sup>th</sup> solar cycles. The ICME number well reproduces the variations of the sunspot numbers. The numbers of GMCs and durations of extreme magnetospheric indices also follow variations of the solar activity, but the curves are not smooth and contain extra peaks in the years of SSN rises and falls. However, all the parameters stay near minima at the minima of solar activity, that is, in intervals 1995–1997, 2006–2010, and 2016–2018.

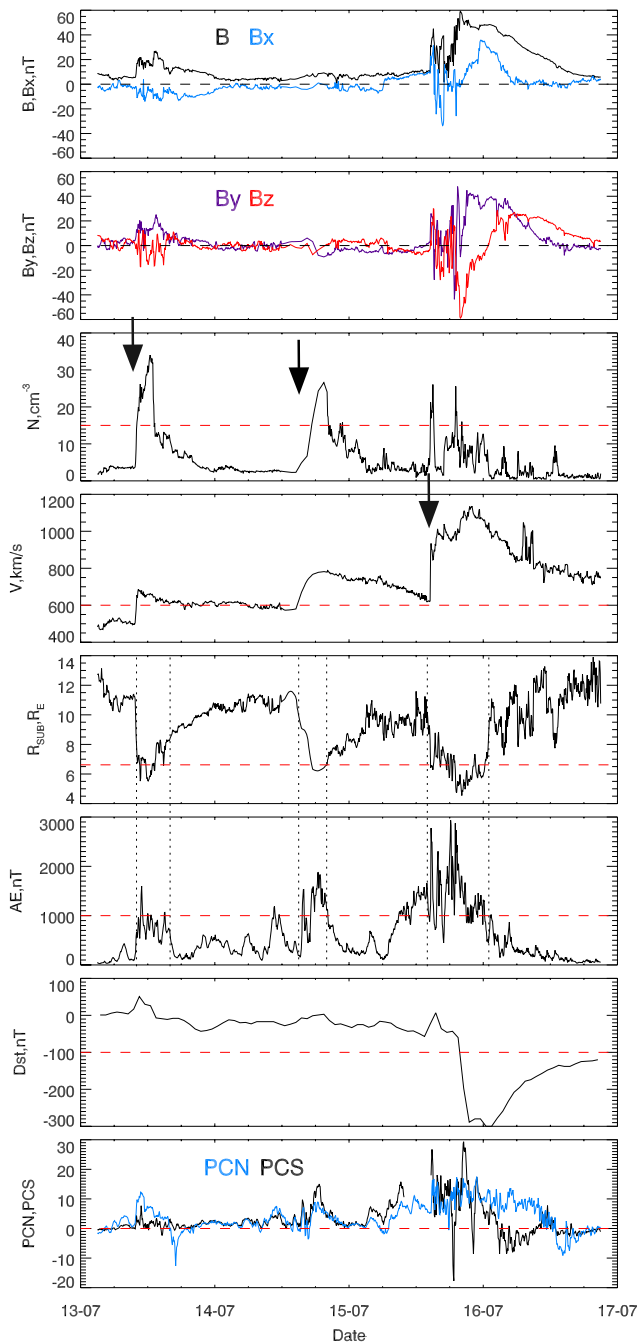


**Figure 2.** July 13–15, 2000 (Bastille Day) event. The interplanetary magnetic field (IMF)  $B$  (black) and  $B_x$  (blue),  $B_y$  (violet), and  $B_z$  (red), the solar wind density and velocity, the magnetopause standoff distance, Dst, AE, and PCN (blue) and PCS (black) indices. The horizontal lines mark  $B = 0$  nT,  $N = 15$   $\text{cm}^{-3}$ , and  $V = 600$  km/s,  $R_{SUB} = 6.62 R_E$ ,  $Dst = -100$  nT,  $AE = 1,000$  nT, and  $PC = 0$ . The dotted vertical lines mark the time intervals of strong magnetospheric compression and corresponding increases in the AE index.

Dst index decreases, but the local Dst minimum during the first ICME is only  $-43$  nT, so the Dst is higher than even in a weak magnetic storm. The second ICME does not cause a magnetic storm either. This may be explained by absence of a long interval with negative  $B_z$  and correspondingly a relatively low total energy

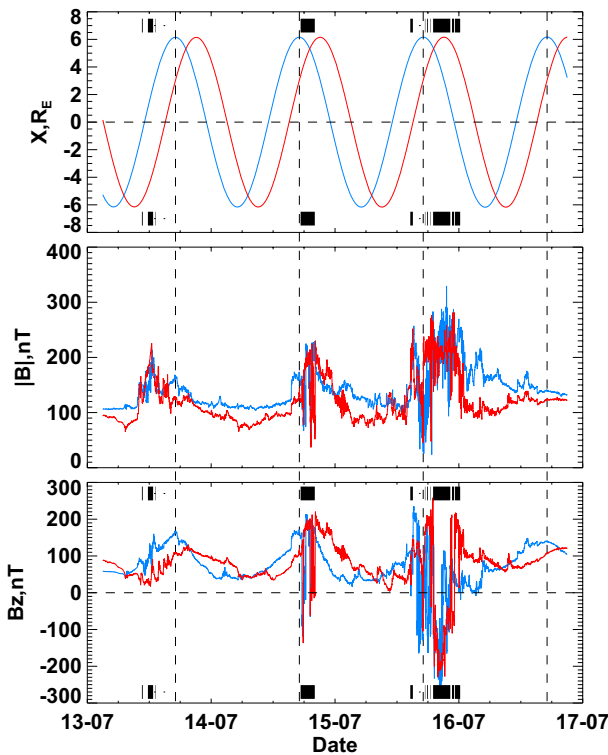
The intervals of high activity in the GMC and ICME numbers and those in the extreme magnetospheric indices mostly coincide but with two exclusions. First, a decrease in the strong SME events in the declining phase of solar cycle is usually one year delayed with respect to the other parameters. Second, we sometimes observe two peaks of the solar and magnetospheric activity numbers near solar maximum with some time lags between the different numbers. For example, in the 24<sup>th</sup> solar cycle, the ICMEs reach two maxima in 2012 and 2014, the GCM events maximize in 2011 and 2015, and the Dst and SME indices maximize in 2012 and 2015. In the 23<sup>rd</sup> solar cycle, two peaks of the GMC numbers in 2000 and 2005 are separated by a significant drop in 2002, while the SSN and CME numbers maximize in 2002. The explanation of these interesting features of the last two solar cycles is beyond the scope of this paper.

#### 4. Magnetospheric Response to GMCs and Confirmation in GOES Data: An Example on July 13–15, 2000

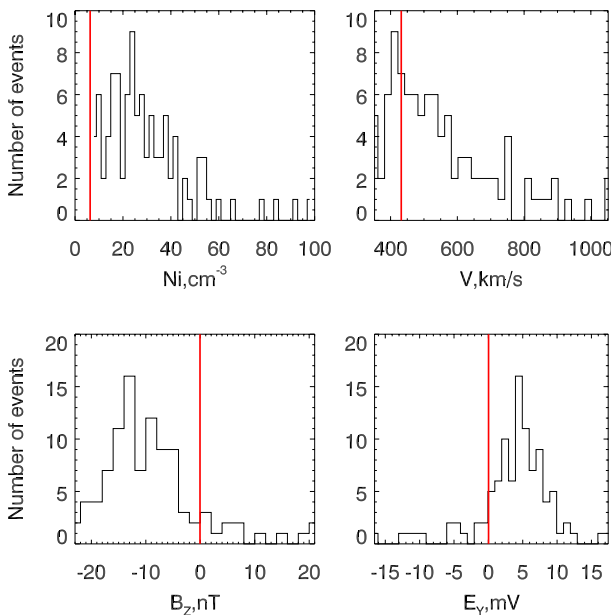
In this section, we compare predictions of the empirical L10 model with GOES observations. This is not a validation of the L10 model, but only an illustration of this study with one specific event. In July 13, 14, and 15, 2000, three successive interplanetary ICMEs encountered the Earth's magnetosphere (Cane & Richardson, 2003). According to the predictions of the L10 model, each of the three ICMEs significantly compressed the magnetosphere and resulted in GMCs (see Table S1 in the Supporting Information). Correspondingly, this event consists of the three “first” GMCs included in our database. Note also that the last ICME results in an extreme geomagnetic storm known as the the Bastille Day Event (Basu et al., 2001; Kil et al., 2003).

Figure 2 shows the IMF magnitude and components, solar wind plasma parameters, the magnetopause standoff distance and magnetospheric indices for the July 13–15, 2000 event. Each ICME begins with increases in the density and velocity. The density grows above  $15$   $\text{cm}^{-3}$  in each pressure pulse, but falls down to several  $\text{cm}^{-3}$  between the pressure pulses. In contrast the velocity stays above the average, near or larger than  $600$  km/s, from the first pressure jump to the end of the interval. The maximal dynamic pressure (not shown) in the first and second pulses is about the same, and becomes higher only at some density peaks in the third pulse. The IMF  $B_z$  fluctuates between negative and positive in the first pressure pulse and keeps relatively close to zero in the second pulse. But the IMF magnitude grows up to  $60$  nT in the third pulse, and a long interval with  $B_z < -10$  nT is observed there.

The behavior of the IMF and solar wind parameters may explain the differences in the magnetospheric response to each ICME. The standoff distance drops below  $6.62 R_E$  in each pressure pulse, but the GMC intervals last only 1–3 h in the first and second pulses. In the third pulse, the interval with GMCs lasts 10 h. The minimal standoff distance predicted by the L10 model is  $4.54 R_E$  at 20:10 UT on July 15. The interplanetary shock at the start of the first ICME results in an increase of the Dst index, that is, the sudden commencement or sudden impulse appears. Then the



**Figure 3.** July 13–15, 2000 (Bastille Day) event. The  $x$  coordinate, magnetic field magnitude, and  $B_z$  in the GSM coordinates from GOES 8 (blue) and GOES 10 (red). The black bars (on the top and bottom panels) indicate the intervals  $R_{SUB} < 6.62 R_E$ .



**Figure 4.** Distribution of hourly solar wind parameters at  $t = 0$  (for first geosynchronous magnetopause crossings [GMCs]). Red vertical lines indicate the average values over the interval 1995–2018.

flux into the magnetosphere. On the contrary, the third ICME results in an extreme magnetic storm, the Bastille Day Event, with a minimum Dst of  $-300$  nT. The storm begins with a storm sudden commencement (SSC). The main phase develops gradually and the Dst index drops below  $-50$  nT only 18 h after the SSC and 19 h after the corresponding GMC. The Dst minimum of  $-300$  nT is reached at 00:30 on July 16, 2000, that is, 29 h after the SSC. The long duration of the storm may be explained by the  $B_z$  behavior. The IMF  $B_z$  is moderately negative for several hours before the SSC, but it becomes extremely negative during the main phase which significantly enhances the energy flux into the magnetosphere. Unlike the Dst index, the AE index exhibits three local maxima each time when the magnetosphere is significantly compressed (the three corresponding time intervals are indicated by vertical lines in Figure 2). Using the SuperMAG indices (Newell & Gjerloev, 2011), we confirm that each of them is a substorm. The third AE increase is highest with the maximum of 2935 nT in the 5 min resolution data. The PC index responds to the pressure pulses in a very similar fashion to the AE index, and each extreme magnetospheric compression coincides with increases in the PC index. The panel shows both the PCN (summer hemisphere) and PCS (winter hemisphere) indices, since the wintertime index is supposed to ensure statistically more correct results (Troshichev & Sormakov, 2019b). In general, the difference between PCN and PCS is minor, except for the third pressure pulse in which the PCS index probably better reproduces the enhanced magnetospheric activity.

The magnetic field data from GOES 8 and 10 at geostationary orbit are also available in this case. In Figure 3, we show the GSM  $x$  coordinate, the magnetic field magnitude and  $B_z$  from both GOES. The black bars mark the time intervals when the L10 model predicts  $R_{SUB} < 6.62 R_E$ . Since the magnetopause standoff distance is smallest near the subsolar point, the GMCs are most likely observed near noon. Although the magnetic field variations at geostationary orbit during magnetospheric compressions may be also observed in the nightside region and near the terminator plane, they are more likely related to global magnetospheric oscillations or substorm dipolarization fronts. Probably the best indicators of GMCs at geostationary orbit are transients of negative  $B_z$  if at least brief intervals of negative  $B_z$  also occur in the solar wind.

In the first GMC interval, both  $|B|$  and  $B_z$  fluctuate but  $B_z$  keeps positive. In the second GMC interval, several pulses of negative  $B_z$  are observed both by GOES 8 and 10. In the third interval, the intervals of  $B_z < 0$  on both spacecraft last several hours and  $B_z$  falls below  $-200$  nT. We conclude that both GOES cross the magnetopause during the second and third intervals because they are close to noon. On the contrary, GOES 8 in the late morning and GOES 10 in the early morning sectors appear to be relatively far from noon to observe the GMCs in the first interval. Instead, GOES observe a compressional wave associated with a maximum of  $|B|$  near 12:00 on July 13. Consequently, GOES observations confirm predictions of the L10 model in this specific case.

## 5. Solar Wind Conditions

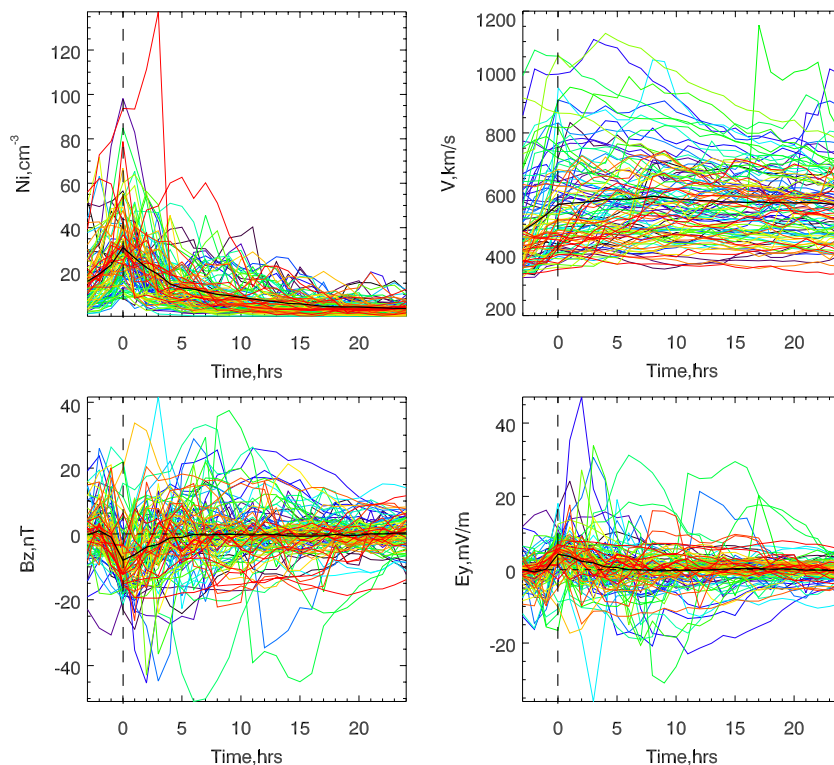
Let us consider the solar wind conditions in the GMC events. In each event, we define the time of first GMC as  $t = 0$ . Figure 4 shows the distribution of hourly solar wind parameters at  $t = 0$  for the list of 99 events.

$N > 10 \text{ cm}^{-3}$	$N > 20 \text{ cm}^{-3}$	$V > 500 \text{ km/s}$	$B_Z < 0$	$B_Z < -5 \text{ nT}$	$E_Y > 2 \text{ mV/m}$
95%	70%	56%	87%	73%	78%

For reference, red vertical lines indicate the corresponding average parameters over the interval 1995–2018:  $N = 6.3 \text{ cm}^{-3}$ ,  $V = 432 \text{ km/s}$ ,  $B_Z = -0.05 \text{ nT}$ , and  $E_Y = 0.03 \text{ mV/m}$  (in GSM coordinates). Evidently, the density and velocity in the GMCs are significantly higher than the averages. The minimal density at  $t = 0$  over all the events is  $7.9 \text{ cm}^{-3}$ , that is, higher than the average over the 24 years. The maximal observed density is  $98 \text{ cm}^{-3}$ , that is, more than one order of magnitude higher than the minimal one. The minimal and maximal velocities in the distribution are 352 and 1,055 km/s respectively, so the velocity is occasionally smaller than the average one. As expected, both  $B_Z$  and  $E_Y$  are approaching zero when averaging over many years. The distributions of  $B_Z$  and  $E_Y$  are asymmetric, that is,  $B_Z$  is mostly negative and  $E_Y$  is positive.

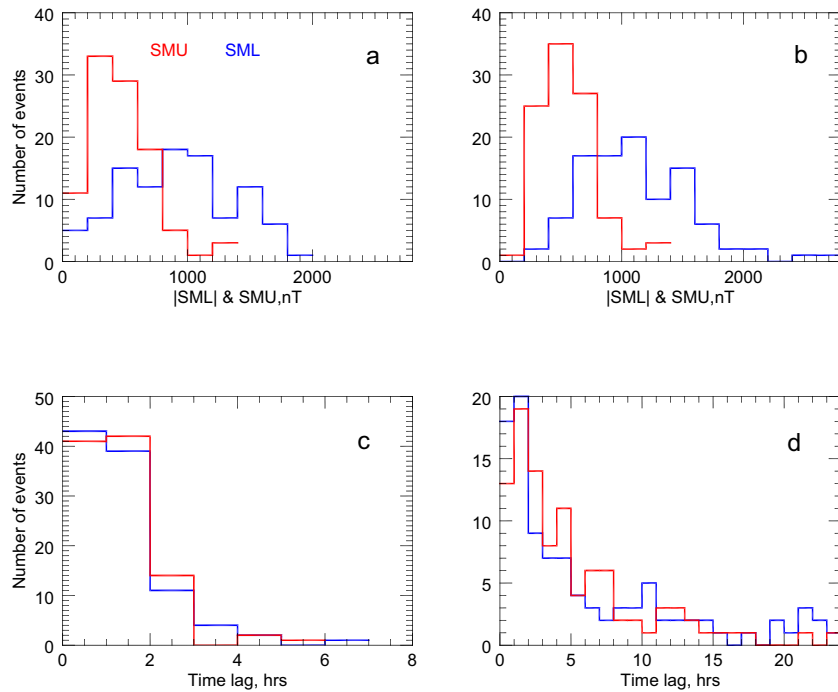
Table 1 quantifies some regularities visible in Figure 4. The density is mostly anomalously increased with 95% events higher than  $10 \text{ cm}^{-3}$  and 70% higher than  $20 \text{ cm}^{-3}$ . The increase in the velocity is not so dramatic, and only 56% events have velocity higher than 500 km/s. The IMF  $B_Z$  is negative in 87%, and strongly negative ( $B_Z < -5 \text{ nT}$ ) in 73%. Respectively, 78% events match the condition  $E_Y > 2 \text{ mV/m}$ . The 13% cases with positive  $B_Z$  occur under extremely strong solar wind dynamic pressure (hourly averages higher than 18 nPa).

Figure 5 displays the evolution of solar wind parameters for the same 99 events in intervals from 3 h before to 24 h after the first GMCs. Individual cases are shown by different colors, while thick black lines correspond to the averages over all GMC events. The results at  $t = 0$  well agree with Figure 4 and Table 1. The pressure pulses at  $t = 0$  are probably more often connected with increases in the density rather than velocity.



**Figure 5.** Solar wind parameters (ion density, velocity, interplanetary magnetic field (IMF)  $B_Z$ , and  $E_Y$ ) in intervals from 3 h before to 24 h after the first geosynchronous magnetopause crossings (GMCs) for all events. Thick black lines indicate average parameters.





**Figure 6.** Distributions of local |SML| (blue) and SMU (red) maxima (a) and (c) and greatest maxima within the next 24 h (b) and (d) (see details in text). Panels (a) and (b) show the largest |SML| and SMU values, panels (c) and (d) display the time lags from the geosynchronous magnetopause crossings (GMCs) to the |SML| and SMU peaks.

At least, the average density demonstrates an evident maximum at  $t = 0$  and then gradually decreases, whereas the average velocity increases before  $t = 0$  and remains large (close to 600 km/s) until the end of the 24 h interval. In each particular case, the density may reach a maximum at  $t = 0$  or several hours later but usually drops down 5–10 h after the first GMC. On the contrary, the velocities in individual events vary from about 350 to 1150 km/s in the 24 h intervals of GMCs, and sometimes may have several maxima with a largest one at any time after  $t = 0$ . Note that the example in the previous section also exhibits such behavior.

The behaviors of  $B_Z$  and  $E_Y$  in Figure 5 are similar to each other, but the average  $B_Z$  has a minimum and the average  $E_Y$  has a maximum at  $t = 0$ . In the next 5 h, both the average  $B_Z$  and  $E_Y$  are approaching zero, while they may reach large negative and positive values in several particular cases.

## 6. Magnetospheric Activity Within the Next 24 h After GMCs

In this section, we analyze magnetospheric activity accompanying and following the GMCs. We begin with studying the time lags between GMC and SMU maximum (SML minimum) which characterize the time of auroral response. Since several SMU maxima (SML minima) may occur in the 24 h interval, we consider two cases. In the first case, we search the local (first after GMC in hourly average data) SMU maxima and SML minima. In the second case, we search greatest SMU maxima (SML minima) within the next 24 h. The histograms in Figure 6 show the magnitudes of SMU (SML) at maxima (minima) and the time lags of the corresponding maxima (minima).

The time lags for local extrema are generally shorter than for largest extrema within the 24 h. In the first case, the time lags do not exceed 6 h, while they are distributed in the whole 24 h interval in the second case. However, most events (82% for SML and 83% for SMU index) occur within one hour after GMCs (this means the GMC hour and the next hour after the GMC) in the first case, and nearly half events occur within two hours after GMCs in the second case. In the first case, 43% events have minimum SML less than  $-1,000$  nT and only 4% events have maximum SMU higher than 1,000 nT. In the second case, SML  $< -1,000$  nT in 57% events and SMU  $> 1,000$  nT in 5%. We obtain similar results for the AE and SME indices (not shown). The behavior of both AE and SME indices demonstrates strong auroral activity a few hours after GMCs too.

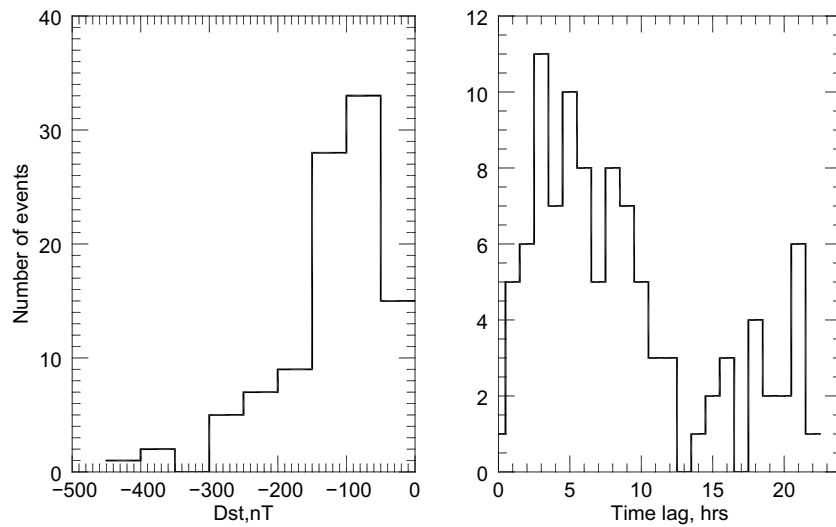


**Figure 7.** Distributions of the greatest Dst minima within the next 24 h.

Figure 7 exhibits the distributions of the Dst index. Here, we present only the greatest minima within the 24 h after GMCs because we assume that the Dst index does not decrease immediately after GMCs and magnetic storms usually need at least several hours to develop. While several substorms (and respectively several SML minima) may occur in the 24 h interval, we usually expect only one magnetic storm for the same 24 h interval. In fact, the corresponding figure with local Dst minima (not shown) displays that the local minima of Dst are even positive ( $Dst > 0$ ) in some cases, but this does not exclude the possibility that a magnetic storm will begin in the next several hours. If we consider a global minimum over the 24 h interval we obtain clear response with a significant Dst decrease. The minimum Dst index falls below  $-50$  nT in 85% of events and below  $-100$  nT in 52% of events. Note that the minimum Dst occurs within the next 12 h in 79% of events. For the distribution function of the time lags in Figure 7, the highest probability of the time lag is 3 h, while the average time lag (or the first moment) equals 8 h.

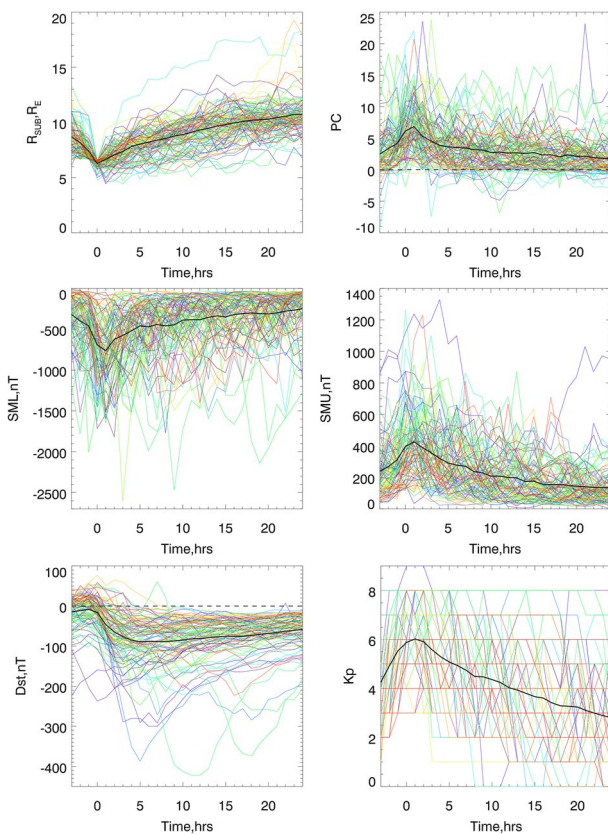


**Figure 8.** Magnetopause standoff distance, PC, SML, SMU, Dst, and  $K_p$  indices in intervals from 3 h before to 24 h after the first geosynchronous magnetopause crossings (GMCs) for all events. Thick black lines indicate average parameters.

Figure 8 displays the variability of magnetospheric response in each event by showing the temporal variations of the predicted magnetopause standoff distance and the indices of magnetospheric activity (PC, SML, SMU, Dst, and  $K_p$ ). Thick black lines on each panel display the averages over all events. The average standoff distance  $R_{SUB}$  has a minimum at  $t = 0$ , since the standoff distance in any event cannot exceed  $6.62 R_E$  at that time by definition. After  $t = 0$ , the standoff distance may immediately increase, may stay below  $6.62 R_E$  for several hours or may increase and then decrease again. We find that the standoff distance stays above  $6.62 R_E$  within the next 24 h in 36% of events, in other words the GMC event consists of only one hour interval. In 20%, the standoff distance is below  $6.62 R_E$  for two hours and then stays above  $6.62 R_E$ . In 38% (38 events), the magnetopause standoff distance drops below six  $R_E$  which means very significant magnetospheric compression.

In Figure 8, we use the wintertime PC index when possible. The PC index is mostly positive in the whole interval with local maxima near  $t = 0$  or, in some cases, later. Interestingly, the average PC peaks at  $t = 1$  h. The time lag between the GMC and minima of SML and maxima of SMU indices agrees with those in Figure 6 and also consists of only one hour

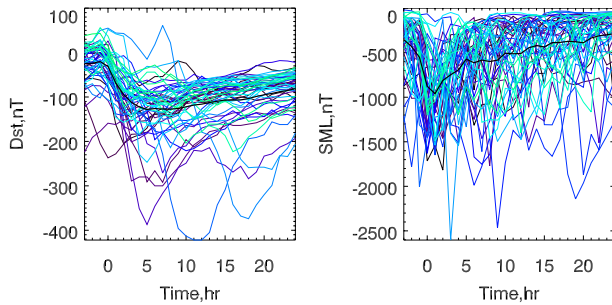


**Figure 9.** Dst and SML indices for the same interval, but only extreme events with hourly Dst <  $-100$  nT and SML <  $-1,100$  nT have been selected. Thick black lines indicate average parameters.

for the average SML and SMU plots. We obtain the same time lags for the average AE and SME (not shown). The minimum average SML equals  $-764$  nT, and the maximum average SMU equals  $426$  nT. Then the average SML (SMU) index gradually increases (decreases), although great local extrema higher than  $-1,000$  ( $1,000$ ) nT occur later, relatively often for the SML index and only in a few events for the SMU index.

The average Dst index decreases after  $t = 0$  and reaches a very smooth minimum of  $-89$  nT at  $t = 5$  h. Since the difference in the average Dst in the interval from 5 to 8 h is less than 1 nT, it would be accurate to say that the time lag of average Dst minimum lies in this interval. As Figure 8 shows, the dispersion of Dst plots is large and Dst minima in each individual case may occur also before and after the interval (5, 8) hours. Note that in addition to the traditional Dst index, we have made the same analysis for the pressure corrected Dst\* (Burton et al., 1975; O'Brien & McPherron, 2000; Wang et al., 2003), but found no significant difference.

Another indicator of the magnetospheric activity is the  $Kp$  index which is typically used in operational space weather activities. The  $Kp$  index here behaves similarly to the SML/SMU indices. In particular, the average  $Kp$  reaches maximum of about 6 at  $t = 1$  h, that is, at the same time as the PC, SML, and SMU indices peak. Note that the  $Kp$  index is 3 h averaged and we can obtain this 1 h time lag only because  $t = 0$  is not synchronized with the 3 h  $Kp$  intervals.

We checked whether the time lags between the GMCs and minima of Dst and SML would depend on strength of the corresponding magnetospheric currents. For this purpose, we select two groups of events, first with minimal Dst <  $-100$  nT (51.5% events) and second with minimal SML <  $-1,100$  nT (49.5% events) within the next 24 h. Figure 9 shows the corresponding Dst and SML plots with the average profiles marked by thick black lines. While the minima of average Dst and SML become smaller than those in Figure 8, the time lags equal 5–8 h (the difference in this interval does not exceed 2 nT) for the Dst index and 1 h for the SML index. The same time lags of the Dst and SML minima have been obtained above for all events, thus the average time lags do not depend on the strength of magnetic storms or substorms at least for this data set.

These results demonstrate that increase in the magnetospheric activity follows the GMCs in most events. We can also find the number of cases when the GMCs are not followed by significant decrease in Dst or increase in SME. We obtain 13 events for which Dst >  $-50$  nT for the next 24 h after GMCs and only one event on July 10, 2015 with Dst >  $-30$  nT. The minimum of Dst in the last event was  $-29$  nT. Likewise, we obtain only five events for which SML >  $-500$  nT; all five events with high SML are included in the list of high Dst (Dst >  $-50$  nT) events. We have inspected these five events and found that four of them are characterized by positive or small negative IMF  $B_z$  after GMCs and only one event has a minimum of  $B_z = -11.6$  nT at  $t = 0$ . Moreover, three of five events were connected with SIR/CIRs in the solar wind (see comparison between ICME and SIR/CIR-related events in the next section). None of the events has minimal SML >  $-300$  nT or maximal SME <  $500$  nT within the next 24 h. Therefore we conclude that the auroral activity always grows at least moderately within the 24 h after the GMCs, and only in one GMC event the upcoming minimum of Dst does not match formally the criteria of magnetic storms, since magnetic storms are defined by condition Dst <  $-30$  nT (Gonzalez et al., 1999).

We would like to learn more about the differences between the GMC events which are followed by strong magnetic storms and by weak or no storms. We select two groups, first with minimal Dst >  $-50$  nT (13 events mentioned above), and second with minimal Dst <  $-100$  nT (51 events also discussed earlier). Figure 10 illustrates the differences in the solar wind dynamic pressure and IMF  $B_z$  between these two groups. We note some typical features of the events with high Dst (weak storms). In these events, the dynamic pressure may significantly increase at  $t = 0$ , but it falls down to a relatively low level in the next several hours, except two cases for which peaks of the pressure higher than 10 nPa occur later. Note that one of these cases is accompanied with a large positive  $B_z$ . As expected, the average  $B_z$  is mostly positive or near zero. Only in three cases the minimum of  $B_z$  at  $t = 0$  falls below  $-10$  nT but  $B_z$  rapidly increases after that. The  $B_z$  in several events during short time intervals drops below  $-5$  nT after  $t = 0$ , but  $|B_z|$  in most cases does not exceed a few nT. On

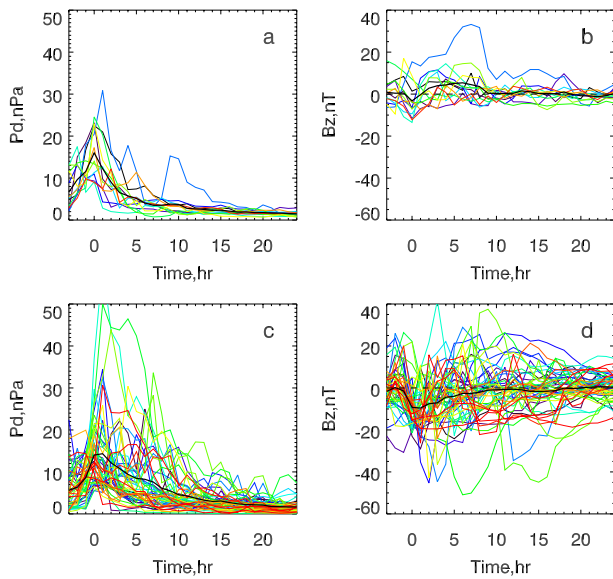


**Figure 10.** The solar wind dynamic pressure (a) and (c) and interplanetary magnetic field (IMF)  $B_z$  (b) and (d) for events with  $Dst > -50$  nT (a) and (b) and with  $Dst \leq -100$  nT (c) and (d). Thick black lines indicate average parameters.

the contrary, the events with low Dst, that is, strong magnetic storms, are characterized by higher magnitude of the IMF  $B_z$ . In several event,  $B_z$  is extremely negative (e.g., below  $-40$  nT), but high positive  $B_z$  are also observed in some cases. Note that the events with low (high) Dst partly coincide with ICME-related (CIR-related) events discussed in the next section.

Since we believe that the estimates of the time lags between GMCs and minimal Dst or minimal SML (maximal SME) are the most important results in our study, we make such estimations with another method in addition to that discussed before, for example, analyzing histograms in Figures 6 and 7. We consider five time intervals within 3/6/12/24/48 h after  $t = 0$  (i.e., the interval 3 h lasts from  $t = 0$  to  $t = 2$  for the hour-averaged data). Then we find minimal Dst or SML during each interval. If the minimal Dst within the 3 h interval coincides with the the minimal Dst within the 6 h interval, we conclude that the response in Dst in this event occurs within the 3 h. If the minimal Dst within the 6 h is less, next we compare the minima within the 6 and 12 h. If these minima coincide, we decide that the response time is 6 h and so on. Here, we use the GMC database of 96 events selected by assuming 48 h response time. We summarize these estimates in Table 2.

Results in Table 2 agree well with the results presented earlier. We remind that the time lag between the GMC and the minimum of average Dst (SML) was found to be equal to 5–8 (1) hours, while the most probable time lag of Dst minima in individual events was 3 h. Now we obtain that the response time falls into the time intervals larger than 3 and smaller than 12 h for 66 (69%) events with minimal Dst while the response time for minimal SML also in 66 events is limited by the 3 h interval. Although this method does not provide accurate time lags, it allows us to partly exclude multiple minima Dst (SML) if several storms or substorms occur during the whole 48 h interval. In this case we would prefer to find the nearest minimum rather than to count the greatest one. However, since the estimates here are consistent with those in the previous subsection we conclude that the time lags obtained above are accurate. Note that we have made the same analysis for the SME index and obtain nearly identical numbers as for the SML index.

### 7. Comparison of Solar Wind Parameters and Magnetospheric Indices Between ICME and CIR/SIR Related Events

Borovsky and Denton (2006) summarized several important differences between CME-driven and CIR-driven magnetic storms, in particular they showed that the CME-driven storms result in stronger response in the Dst index and can produce greater auroral activity. In this study, we found that 74 GMC events are connected with ICMEs and 18 events are connected with SIR/CIRs. Even though the number of SIR/CIRs is nearly 4 times less than the number of ICMEs, it is possible to compare the average solar wind and magnetospheric parameters for the two types of events.

Figure 11 shows the solar wind dynamic pressure, density, velocity, and IMF  $B_z$  for the ICMEs (left panels) and SIR/CIRs (right panels). As expected, some ICMEs are characterized by great increase in the dynamic pressure and/or IMF  $B_z$  that eventually results in extreme magnetospheric compression in several cases (see Figure 12 below). However, the differences between average  $Pd$  and  $B_z$  are relatively small, for example, the

average  $Pd$  at  $t = 0$  is 14.9 nPa for ICMEs and 13.8 nPa for SIR/CIRs, and  $B_z$  is  $-8.3$  nT for ICMEs and  $-7.0$  nT for SIR/CIRs (see also Table 3). On the contrary, the differences between average density and velocity near  $t = 0$  are evident. The density is higher for SIR/CIRs and the velocity is higher for ICMEs, in particular the average  $V$  is 599 km/s for ICMEs and 432 km/s for SIR/CIRs. As we obtain above for all events, the average density has a peak at  $t = 0$  and then decreases for both ICMEs and SIR/CIRs. The average velocity for ICMEs after  $t = 0$  keeps nearly constant for several hours and then slightly decreases. The velocity for SIR/CIRs

**Table 2**  
Time Lags Between “First” GMCs and Magnetospheric Response in Minimal Dst and SML (See Details in Text)

Time (hr)	3	6	12	24	48
Number of Dst events	16	33	33	13	1
Number of SML events	66	21	4	3	2

Abbreviation: GMC, geosynchronous magnetopause crossing



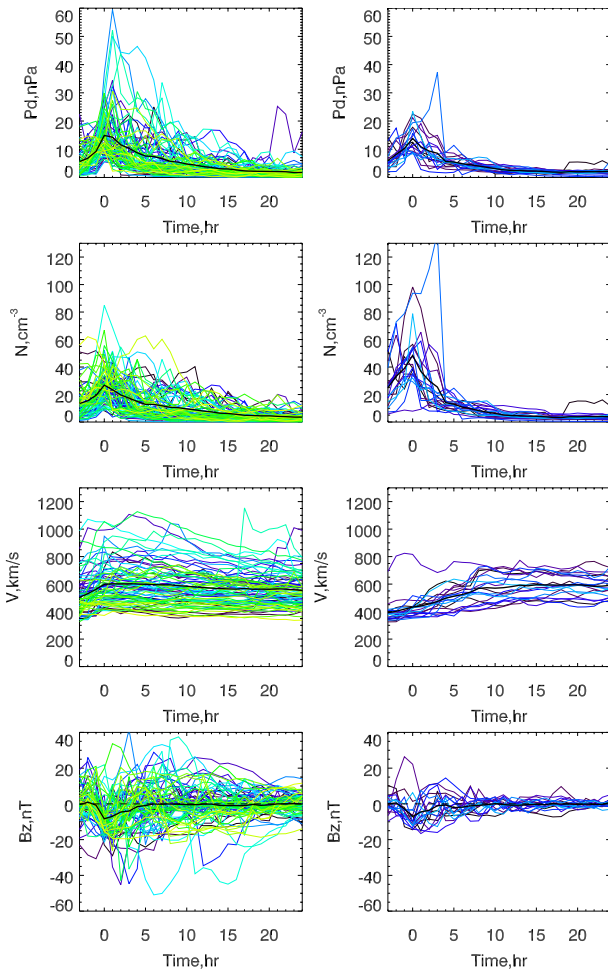


**Figure 11.** The solar wind dynamic pressure, density, velocity, and interplanetary coronal mass ejections (IMF)  $B_z$  for interplanetary coronal mass ejections (ICME)-related (left) and corotating interaction regions (CIR)-related (right) events. Thick black lines indicate average parameters.

increases for several hours after  $t = 0$  and then keeps nearly constant as expected for the interface region between the slow and fast solar wind.

Figure 12 shows the magnetopause standoff distance, magnetospheric Dst, SML, and  $K_p$  indices for ICMEs and SIR/CIRs. Since both the average dynamic pressure and  $B_z$  slightly differ between ICMEs and SIR/CIRs, the average magnetospheric compression is only a little stronger for ICMEs ( $R_{SUB} = 6.24 R_E$ ) than for SIR/CIRs ( $R_{SUB} = 6.38 R_E$ ) and the minimum in both the cases is at  $t = 0$ . The shape of the average curves is also very similar for ICMEs and SIR/CIRs, that is, the rate of magnetospheric expansion after the compressions is about the same. Contrary to the standoff distance, the differences in the magnetospheric indices become more obvious. The minimal average Dst is  $-100$  nT for ICMEs (at  $t = 5$  h) and  $-59$  nT for SIR/CIRs (at  $t = 8$  h), the minimal SML is  $-835$  nT for ICMEs and  $-546$  nT for SIR/CIRs (both at  $t = 1$  h), the maximal  $K_p$  is 6.3 for ICMEs (at  $t = 1$  h) and 5.3 for SIR/CIRs (at  $t = 2$  h). In Table 3, we show the average magnetospheric indices for ICMEs and SIR/CIRs observed at the same times for comparison (see caption to the table) therefore the numbers of Dst and  $K_p$  for SIR/CIRs in the table are different from those in the text.

Our analysis shows that ICME events are characterized both by stronger ring current and enhanced auroral activity in comparison with SIR/CIR events. This agrees with previous studies (e.g., Alves et al., 2011; Borovsky & Denton, 2006; Yermolaev et al., 2010) which mostly show that sheaths (compressed regions before ICME) and/or magnetic clouds are more geoeffective than CIRs. In this paper, we use a completely different selection criteria than in the other studies, because we focus on the GMC events and synchronize all events with the times of first GMC. We find that despite the average solar wind dynamic pressures are close to each other for ICMEs and CIRs, the average density and velocity differ for the two groups of events. The density increases at  $t = 0$  in both ICME and CIR-related events, while the velocity increases at  $t = 0$  only in the ICME-related events. The velocity in the CIR-related events usually grows smoothly after density decline. The magnetic field in the ICME and CIR-related events may differ in each particular case, but the average  $B_z$  looks rather similar. Therefore we suggest that the different velocity behavior may explain the difference in the consequent magnetospheric activity in response to ICMEs and SIR/CIRs.

## 8. Conclusions

Many extreme magnetospheric events begin with strong magnetospheric compression. In this paper, we collect GMC events using the empirical magnetopause model (Lin et al., 2010). Selecting “first” GMC in the 24 h intervals, we make a list of 99 events from 1995 to 2018. We describe the solar wind conditions responsible for the GMCs and study the magnetospheric response in terms of magnetospheric indices. We demonstrate that all the GMC events are followed by an increase in magnetospheric activity. We highlight some results below.

1. The number of GMCs each year generally follows the solar activity, but the peaks of GMCs as well as the peaks of extreme Dst and SME indices may not coincide with the peaks of sunspot numbers.
2. Using ICME and CIR catalogs, we classify 74 (of 99) events as ICMEs and 18 events as SIR/CIRs. Furthermore, we have found that 76 GMCs follow IP shocks. If we combine all solar wind structures (ICMEs, SIR/CIRs, and IP shocks) together, we obtain that all the GMCs are connected with at least one of the solar wind disturbances identified by the catalogs. We conclude that the GMCs mostly follow ICMEs and IP shocks. In 63 events, strong compression lasts more than 1 h.

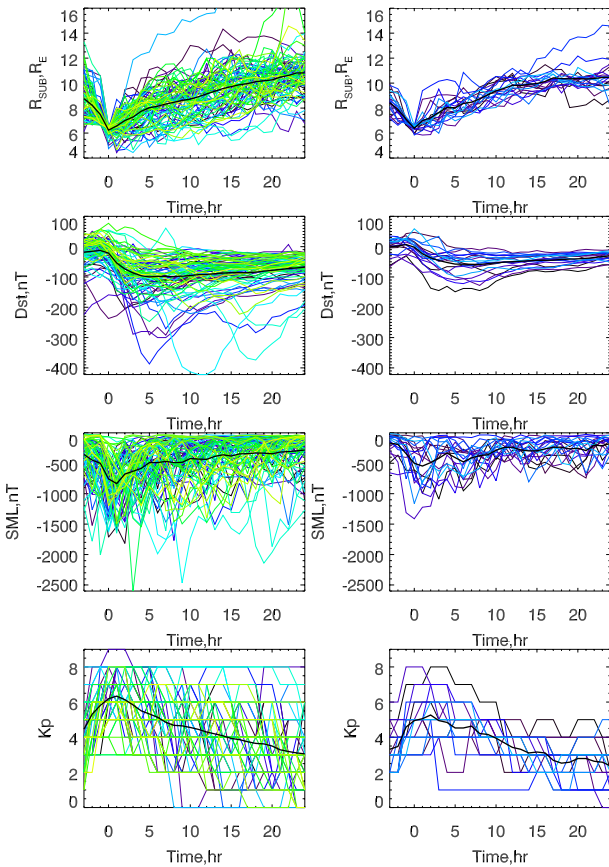


**Figure 12.** The magnetopause standoff distance, Dst, SML, and  $K_p$  indices for interplanetary coronal mass ejections (ICME)-related (left) and CIR-related (right) events. Thick black lines indicate average parameters.

3. Two factors result in a magnetospheric compression: an increase in the solar wind dynamic pressure and a decrease in the IMF  $B_z$ . In turn, a pulse of the solar wind dynamic pressure may be caused by increases in the density or velocity. The density often increases twice or more at the pressure pulse, but decreases several hours later. On the contrary, the hourly averaged velocity usually increases only by 5%–40% before or at the first GMCs ( $t = 0$ ), but remains enlarged and may have several maxima later, in the 24-h intervals after the first GMC. At  $t = 0$ , the density is higher than  $10 \text{ cm}^{-3}$  in 95% cases and higher than  $20 \text{ cm}^{-3}$  in 70% cases, while the velocity is higher than 500 km/s in 56% cases. Accordingly, the dynamic pressure pulse at the first GMC mostly results from a strong enhancement of the density.
4. The average IMF  $B_z$  is negative at the first GMC, but it approaches zero several hours later.  $B_z$  may vary between strongly negative and strongly positive values in each particular case, but it is negative at  $t = 0$  in 87% cases. Moreover,  $B_z$  is strongly negative ( $< -5 \text{ nT}$ ) at  $t = 0$  in 73% cases.
5. The average PC, SMU (SML), and  $K_p$  indices reach maxima (minimum) in 1 h after  $t = 0$ , while the average Dst index reaches a smooth minimum in 5–8 h after  $t = 0$ . The local SML minimum occurs in 0–2 h after GMC in 93% cases, while the greatest SML minimum in the 24 h interval occurs in 0–5 h in 66% cases. The greatest Dst minimum in the 24 h interval occurs in 1–10 h after GMC in 73% cases. The SML minimum is less than  $-500 \text{ nT}$  in the next 24 h in 95% cases and less than  $-300 \text{ nT}$  in 100% cases. The maximum of SME index is higher than 500 nT in all cases too. The Dst minimum is less than  $-30 \text{ nT}$  in 99% cases. Consequently, we conclude that the GCM events are mostly followed by strong substorms and at least weak magnetic storms in the next 24 h.
6. We obtain the same time lags between the first GMC and the minimum of Dst (minimum of SML) for strong magnetic storms with  $\text{Dst} < -100 \text{ nT}$  (strong substorms with  $\text{SML} < -1,100 \text{ nT}$ ) as for the whole data set showing that the time lags do not depend on the storm (substorm) strength.
7. We compare solar wind and magnetospheric conditions for the GMCs connected with either ICMEs or SIR/CIRs. The difference in the solar wind dynamic pressure and IMF  $B_z$  between the two groups is relatively small, however the solar wind density and velocity are noticeably different at  $t = 0$ . The density is higher for SIR/CIRs, and the velocity is higher for ICMEs. The average magnetopause standoff distance at  $t = 0$  is insignificantly smaller for ICMEs, but magnetospheric activity in terms of the average magnetospheric indices Dst, SML, and  $K_p$  is appreciably higher for ICMEs, for example, the minimal average Dst after GMC is  $-100 \text{ nT}$  for ICMEs and  $-59 \text{ nT}$  for SIR/CIRs, and the minimal SML is  $-835 \text{ nT}$  for ICMEs and  $-546 \text{ nT}$  for SIR/CIRs. Previous studies (e.g., Borovsky & Denton, 2006) have already shown that ICME-related magnetic storms are characterized by stronger ring current and auroral activity, but

**Table 3**

Average Solar Wind Parameters and Magnetospheric Indices for ICME and SIR/CIR Data Sets at  $t = 0$  (Solar Wind Parameters and  $R_{\text{SUB}}$ ),  $t = 5 \text{ h}$  (Dst), and  $t = 1 \text{ h}$  (SML,  $K_p$ )

Parameters	Pd nPa	$\text{N cm}^{-3}$	V km/s	BZ nT	R <sub>SUB</sub> RE	Dst nT	SML nT	$K_p$
ICMEs	14.9	27	599	-8.3	6.24	-100	-835	6.3
SIR/CIRs	13.8	48	432	-7.0	6.38	-58	-546	5.1

Abbreviations: CIR, corotating interaction regions; ICME, interplanetary coronal mass ejections; SIR, stream interaction regions.

using our data set we suggest that this might be explained by higher solar wind velocity at the time of greatest compression. The larger velocity for southward IMF (that occurs in most GMC events) results in the higher magnetopause reconnection rate and correspondingly in the higher energy flux into the magnetosphere (e.g., Perreault & Akasofu, 1978).

We selected GMC events using Lin et al. (2010)'s model rather than in-situ observations and we have several reasons for this choice. First, Lin et al (2010)'s model well agrees with observations at geostationary orbit and demonstrates better results than other empirical models (Dmitriev et al., 2016). We check predictions of the L10 model using GOES data for one year, 2005, and confirm that the model agrees well with the observations. Using an empirical model, we can obtain a continuous data set of the magnetopause standoff distance based on the solar wind conditions, while direct observations give a very scattered set of GMCs. Second, the results of this work indirectly confirm a good predictability of extreme events because we connect all the GMC events with the corresponding solar wind disturbances.

Finally, we note that 534 active satellites were located on geostationary orbit on January 4, 2021 according to <https://www.satsig.net/sslist.htm> therefore predictions of GMC events are an important space weather problem. Usually, the prediction of GMCs requires only the information about solar wind conditions, contrary to the prediction of magnetic storms and substorms which requires either the knowledge of the history of solar wind conditions or the information about the energy accumulated in the magnetosphere or both. Consequently, we believe that it is easier to predict GMCs than storms or substorms. When GMC occurs, we expect that a substorm will begin in the next two hours and a magnetic storm (Dst minimum) with a high probability will occur in the next 10 h. In each particular case, however, this rule may apply differently. We consider in details an event on July 13–15, 2000 when three successive ICMEs encountered the magnetosphere. Each ICME triggers a substorm, but only the last ICME results in a magnetic storm. Predictions of GMCs can be validated not only by GEO satellites, but also by future imaging missions, such as SMILE.

### Data Availability Statement

The OMNI data are available from Coordinated Data Analysis Web (CDAWeb), <http://cdaweb.gsfc.nasa.gov>. GOES magnetic field data are available from CDAWeb and National Oceanic and Atmospheric Administration (NOAA), <http://ngdc.noaa.gov>. The access to the SOHO LASCO CME Catalog is available through the CDAWeb data center. The near-Earth ICME catalog is available at <http://www.srl.caltech.edu/ACE/ASC/DATA/level3/icmetable2.htm>. The STEREO SIR/CIR observations are available at [https://www.helcats-fp7.eu/catalogues/wp5\\_cat.html](https://www.helcats-fp7.eu/catalogues/wp5_cat.html). The other CIR/SIR catalogs were published by (Jian et al., 2006) and (Zhang et al., 2007). The IP shocks data were obtained from (Oliveira & Raeder, 2015) and online from the Harvard-Smithsonian center <https://www.cfa.harvard.edu/shocks/>.

### References

- Adams, W. G. (1892). Comparison of simultaneous magnetic disturbances at several observatories. *Philosophical Transactions of the Royal Society A*, 183, 131–140. <https://doi.org/10.1098/rsta.1892.0004>
- Alves, M., Echer, E., & Gonzalez, W. (2011). Geoeffectiveness of solar wind interplanetary magnetic structures. *Journal of Atmospheric and Solar-Terrestrial Physics*, 73(11), 1380–1384. <https://doi.org/10.1016/j.jastp.2010.07.024>
- Aubry, M. P., & McPherron, R. L. (1971). Magnetotail changes in relation to the solar wind magnetic field and magnetospheric substorms. *Journal of Geophysical Research*, 76(19), 4381–4401. <https://doi.org/10.1029/JA076i019p04381>
- Bartels, J. (1949). The standardized index Ks and the planetary index Kp, *iatme bull.* 126, 97. Paris: Publication Office
- Basu, S., Basu, S., Groves, K. M., Yeh, H.-C., Su, S.-Y., Rich, F. J., et al. (2001). Response of the equatorial ionosphere in the south atlantic region to the great magnetic storm of July 15, 2000. *Geophysical Research Letters*, 28(18), 3577–3580. <https://doi.org/10.1029/2001GL013259>
- Borovsky, J. E., & Denton, M. H. (2006). Differences between cme-driven storms and cir-driven storms. *Journal of Geophysical Research*, 111(A7), A07S08. <https://doi.org/10.1029/2005JA011447>
- Burch, J. L. (1972). Preconditions for the triggering of polar magnetic substorms by storm sudden commencements. *Journal of Geophysical Research*, 77(28), 5629–5632. <https://doi.org/10.1029/JA077i028p05629>
- Burton, R. K., McPherron, R. L., & Russell, C. T. (1975). An empirical relationship between interplanetary conditions and dst. *Journal of Geophysical Research*, 80(31), 4204–4214. <https://doi.org/10.1029/JA080i031p04204>
- Cane, H. V., & Richardson, I. G. (2003). Interplanetary coronal mass ejections in the near-Earth solar wind during 1996–2002. *Journal of Geophysical Research*, 108(A4), 1156. <https://doi.org/10.1029/2002JA009817>
- Dmitriev, A. V., Lin, R. L., Liu, S. Q., & Suvorova, A. V. (2016). Model prediction of geosynchronous magnetopause crossings. *Space Weather*, 14(8), 530–543. <https://doi.org/10.1002/2016SW001385>
- Dmitriev, A. V., & Suvorova, A. V. (2000). Three-dimensional artificial neural network model of the dayside magnetopause. *Journal of Geophysical Research*, 105(A8), 18909–18918. <https://doi.org/10.1029/2000JA900008>

### Acknowledgments

The authors thank Prof. Mike Hapgood for a valuable consultation on the space weather effects on the satellites outside of the magnetosphere. The authors express gratitude to Ian Richardson for a consultation on ICME events from their catalog. A.A.Samsonov and G.Branduardi-Raymont acknowledge support from the UK Space Agency under grant ST/T002964/1. Y.V.Bogdanova is supported by the STFC RAL Space IHR grant.

- Echer, E., Tsurutani, B. T., Guarnieri, F. L., & Kozyra, J. U. (2011). Interplanetary fast forward shocks and their geomagnetic effects: CAUSES events. *Journal of Atmospheric and Solar-Terrestrial Physics*, 73(11–12), 1330–1338. <https://doi.org/10.1016/j.jastp.2010.09.020>
- Gjerloev, J. W. (2012). The supermag data processing technique. *Journal of Geophysical Research*, 117(A9), A09213. <https://doi.org/10.1029/2012JA017683>
- Gonzalez, W. D., Tsurutani, B. T., & Clúa de Gonzalez, A. L. (1999). Interplanetary origin of geomagnetic storms. *Space Science Reviews*, 88(3), 529–562. <https://doi.org/10.1023/A:1005160129098>
- Gosling, J. T., McComas, D. J., Phillips, J. L., & Bame, S. J. (1991). Geomagnetic activity associated with earth passage of interplanetary shock disturbances and coronal mass ejections. *Journal of Geophysical Research*, 96(A5), 7831–7839. <https://doi.org/10.1029/91JA00316>
- Henderson, M. G., Reeves, G. D., Belian, R. D., & Murphree, J. S. (1996). Observations of magnetospheric substorms occurring with no apparent solar wind/imf trigger. *Journal of Geophysical Research*, 101(A5), 10773–10791. <https://doi.org/10.1029/96JA00186>
- Horwitz, J. L. (1985). The substorm as an internal magnetospheric instability: Substorms and their characteristic time scales during intervals of steady interplanetary magnetic field. *Journal of Geophysical Research*, 90(A5), 4164–4170. <https://doi.org/10.1029/JA090iA05p04164>
- Jian, L., Russell, C. T., Luhmann, J. G., & Skoug, R. M. (2006). Properties of stream interactions at one au during 1995–2004. *Solar Physics*, 239, 337–392. <https://doi.org/10.1007/s11207-006-0132-3>
- Joselyn, J. A., & Tsurutani, B. T. (1990). Geomagnetic sudden impulses and storm sudden commencements: A note on terminology. *Eos, Transactions American Geophysical Union*, 71(47), 1808–1809. <https://doi.org/10.1029/90EO00350>
- Keika, K., Nakamura, R., Baumjohann, W., Angelopoulos, V., Chi, P. J., Glassmeier, K. H., et al. (2009). Substorm expansion triggered by a sudden impulse front propagating from the dayside magnetopause. *Journal of Geophysical Research*, 114(A1), A00C24. <https://doi.org/10.1029/2008JA013445>
- Kil, H., Paxton, L. J., Pi, X., Hairston, M. R., & Zhang, Y. (2003). Case study of the 15 July 2000 magnetic storm effects on the ionosphere-driver of the positive ionospheric storm in the winter hemisphere. *Journal of Geophysical Research*, 108(A11), 1391. <https://doi.org/10.1029/2002JA009782>
- Kokubun, S., McPherron, R. L., & Russell, C. T. (1977). Triggering of substorms by solar wind discontinuities. *Journal of Geophysical Research*, 82(1), 74–86. <https://doi.org/10.1029/JA082i001p00074>
- Lin, R. L., Zhang, X. X., Liu, S. Q., Wang, Y. L., & Gong, J. C. (2010). A three-dimensional asymmetric magnetopause model. *Journal of Geophysical Research*, 115, A04207. <https://doi.org/10.1029/2009JA014235>
- Liou, K., Newell, P. T., Meng, C.-I., Wu, C.-C., & Lepping, R. P. (2003). Investigation of external triggering of substorms with polar ultraviolet imager observations. *Journal of Geophysical Research*, 108(A10). <https://doi.org/10.1029/2003JA009984>
- Lyons, L. R., Lee, D.-Y., Wang, C.-P., & Mende, S. B. (2005). Global auroral responses to abrupt solar wind changes: Dynamic pressure, substorm, and null events. *Journal of Geophysical Research*, 110(A8), A08208. <https://doi.org/10.1029/2005JA011089>
- McPherron, R. L., Terasawa, T., & Nishida, A. (1986). Solar wind triggering of substorm expansion onset. *Journal of Geomagnetism and Geoelectricity*, 38(11), 1089–1108. <https://doi.org/10.5636/jgg.38.1089>
- Morley, S. K., & Freeman, M. P. (2007). On the association between northward turnings of the interplanetary magnetic field and substorm onsets. *Geophysical Research Letters*, 34(8), L08104. <https://doi.org/10.1029/2006GL028891>
- Nemecek, Z., Safrankova, J., Lopez, R., Dusik, S., Nouzak, L., Prech, L., et al. (2016). Solar cycle variations of magnetopause locations. *Advances in Space Research*, 58(2), 240–248. <https://doi.org/10.1016/j.asr.2015.10.012>
- Newell, P. T., & Gjerloev, J. W. (2011). Evaluation of supermag auroral electrojet indices as indicators of substorms and auroral power. *Journal of Geophysical Research*, 116(A12), A12211. <https://doi.org/10.1029/2011JA016779>
- Newell, P. T., Sotirelis, T., Liou, K., Meng, C.-I., & Rich, F. J. (2007). A nearly universal solar wind-magnetosphere coupling function inferred from 10 magnetospheric state variables. *Journal of Geophysical Research*, 112(A1), A01206. <https://doi.org/10.1029/2006JA012015>
- Nose, M., Sugiura, M., Kamei, T., Iyemori, T., & Koyama, Y. (2015). *Dst index*. Kyoto: WDC for Geomagnetism. <https://doi.org/10.17593/14515-74000>
- O'Brien, T., & McPherron, R. L. (2000). Forecasting the ring current index dst in real time. *Journal of Atmospheric and Solar-Terrestrial Physics*, 62(14), 1295–1299. [https://doi.org/10.1016/S1364-6826\(00\)00072-9](https://doi.org/10.1016/S1364-6826(00)00072-9)
- Olifer, L., Mann, I. R., Ozeke, L. G., Rae, I. J., & Morley, S. K. (2019). On the relative strength of electric and magnetic ulf wave radial diffusion during the march 2015 geomagnetic storm. *Journal of Geophysical Research: Space Physics*, 124(4), 2569–2587. <https://doi.org/10.1029/2018JA026348>
- Oliveira, D. M., & Raeder, J. (2015). Impact angle control of interplanetary shock geoeffectiveness: A statistical study. *Journal of Geophysical Research: Space Physics*, 120(6), 4313–4323. <https://doi.org/10.1002/2015JA021147>
- Perreault, P., & Akasofu, S. I. (1978). A study of geomagnetic storms. *Geophysical Journal International*, 54(3), 547–573. <https://doi.org/10.1111/j.1365-246X.1978.tb05494.x>
- Petrinec, S. M., & Russell, C. T. (1996). Near-Earth magnetotail shape and size as determined from the magnetopause flaring angle. *Journal of Geophysical Research*, 101, 137–152. <https://doi.org/10.1029/95JA02834>
- Raab, W., Branduardi-Raymont, G., Dai, L., Wang, C., Donovan, E., Enno, G., et al. (2016). Smile: A joint esa/cas mission to investigate the interaction between the solar wind and earth's magnetosphere. In *Space telescopes and instrumentation 2016: Ultraviolet to gamma ray*. *Proceedings of SPIE*. 9905, 990502. <https://doi.org/10.1117/12.2231984>
- Richardson, I. G. (2018). Solar wind stream interaction regions throughout the heliosphere. *Living Reviews in Solar Physics*, 15, 1. <https://doi.org/10.1007/s41116-017-0011-z>
- Richardson, I. G., & Cane, H. V. (2010). Near-earth interplanetary coronal mass ejections during solar cycle 23 (1996–2009): Catalog and summary of properties. *Solar Physics*, 264(1), 189–237. <https://doi.org/10.1007/s11207-010-9568-6>
- Rostoker, G. (1983). Triggering of expansive phase intensifications of magnetospheric substorms by northward turnings of the interplanetary magnetic field. *Journal of Geophysical Research*, 88(A9), 6981–6993. <https://doi.org/10.1029/JA088iA09p06981>
- Samsonov, A. A., Bogdanova, Y. V., Branduardi-Raymont, G., Safrankova, J., Nemecek, Z., & Park, J.-S. (2019). Long-term variations in solar wind parameters, magnetopause location, and geomagnetic activity over the last five solar cycles. *Journal of Geophysical Research: Space Physics*, 124(6), 4049–4063. <https://doi.org/10.1029/2018JA026355>
- Samsonov, A. A., Bogdanova, Y. V., Branduardi-Raymont, G., Sibeck, D. G., & Toth, G. (2020). Is the relation between the solar wind dynamic pressure and the magnetopause standoff distance so straightforward? *Geophysical Research Letters*, 47(8), e2019GL086474. <https://doi.org/10.1029/2019GL086474>
- Samsonov, A. A., Gordeev, E., Tsyganenko, N. A., Šafránková, J., Němeček, Z., Šimunek, J., et al. (2016). Do we know the actual magnetopause position for typical solar wind conditions? *Journal of Geophysical Research*, 121, 6493–6508. <https://doi.org/10.1002/2016JA022471>
- Shue, J.-H., Song, P., Russell, C. T., Steinberg, J. T., Chao, J. K., Zastenker, G., et al. (1998). Magnetopause location under extreme solar wind conditions. *Journal of Geophysical Research*, 103, 17691–17700. <https://doi.org/10.1029/98JA01103>



- Sibeck, D. G., Lopez, R. E., & Roelof, E. C. (1991). Solar wind control of the magnetopause shape, location, and motion. *Journal of Geophysical Research*, 96(A4), 5489–5495. <https://doi.org/10.1029/90JA02464>
- Smith, A. W., Rae, I. J., Forsyth, C., Oliveira, D. M., Freeman, M. P., & Jackson, D. R. (2020). Probabilistic forecasts of storm sudden commencements from interplanetary shocks using machine learning. *Space Weather*, 18(11), e2020SW002603. <https://doi.org/10.1029/2020SW002603>
- Sonett, C. P., Colburn, D. S., Davis, L., Smith, E. J., & Coleman, P. J. (1964). Evidence for a collision-free magnetohydrodynamic shock in interplanetary space. *Physical Review Letters*, 13, 153–156. <https://doi.org/10.1103/PhysRevLett.13.153>
- Staples, F. A., Rae, I. J., Forsyth, C., Smith, A. R. A., Murphy, K. R., Raymer, K. M., et al. (2020). Do statistical models capture the dynamics of the magnetopause during sudden magnetospheric compressions? *Journal of Geophysical Research: Space Physics*, 125(4), e2019JA027289. <https://doi.org/10.1029/2019JA027289>
- Troshichev, O., Andrezen, V., Vennerström, S., & Friis-Christensen, E. (1988). Magnetic activity in the polar cap—A new index. *Planetary and Space Science*, 36(11), 1095–1102. [https://doi.org/10.1016/0032-0633\(88\)90063-3](https://doi.org/10.1016/0032-0633(88)90063-3)
- Troshichev, O. A., & Andrezen, V. G. (1985). The relationship between interplanetary quantities and magnetic activity in the southern polar cap. *Planetary and Space Science*, 33(4), 415–419. [https://doi.org/10.1016/0032-0633\(85\)90086-8](https://doi.org/10.1016/0032-0633(85)90086-8)
- Troshichev, O. A., Podorozhkina, N. A., Sormakov, D. A., & Janzhura, A. S. (2014). Pc index as a proxy of the solar wind energy that entered into the magnetosphere: Development of magnetic substorms. *Journal of Geophysical Research: Space Physics*, 119(8), 6521–6540. <https://doi.org/10.1002/2014JA019940>
- Troshichev, O. A., & Sormakov, D. A. (2019a). Pc index as a proxy of the solar wind energy that entered into the magnetosphere: 4. Relationship between the solar wind dynamic pressure (psw) impulses and pc, al indices. *Journal of Atmospheric and Solar-Terrestrial Physics*, 182, 200–210. <https://doi.org/10.1016/j.jastp.2018.12.001>
- Troshichev, O. A., & Sormakov, D. A. (2019b). Pc index as a proxy of the solar wind energy that entered into the magnetosphere: 5. Verification of the solar wind parameters presented at omni website. *Journal of Atmospheric and Solar-Terrestrial Physics*, 196, 105147. <https://doi.org/10.1016/j.jastp.2019.105147>
- Tsurutani, B. T., Gonzalez, W. D., Tang, F., Akasofu, S. I., & Smith, E. J. (1988). Origin of interplanetary southward magnetic fields responsible for major magnetic storms near solar maximum (1978–1979). *Journal of Geophysical Research*, 93(A8), 8519–8531. <https://doi.org/10.1029/JA093iA08p08519>
- Tu, W., Xiang, Z., & Morley, S. K. (2019). Modeling the magnetopause shadowing loss during the June 2015 dropout event. *Geophysical Research Letters*, 46(16), 9388–9396. <https://doi.org/10.1029/2019GL084419>
- Turner, D. L., Shprits, Y., Hartinger, M., & Angelopoulos, V. (2012). Explaining sudden losses of outer radiation belt electrons during geomagnetic storms. *Nature Physics*, 8(3), 208–212. <https://doi.org/10.1038/nphys2185>
- Vokhmyanin, M. V., Stepanov, N. A., & Sergeev, V. A. (2019). On the evaluation of data quality in the omni interplanetary magnetic field database. *Space Weather*, 17(3), 476–486. <https://doi.org/10.1029/2018SW002113>
- Wang, C. B., Chao, J. K., & Lin, C.-H. (2003). Influence of the solar wind dynamic pressure on the decay and injection of the ring current. *Journal of Geophysical Research*, 108(A9), 1341. <https://doi.org/10.1029/2003JA009851>
- Wang, Y., Sibeck, D. G., Merka, J., Boardsen, S. A., Karimabadi, H., Sipes, T. B., et al. (2013). A new three-dimensional magnetopause model with a support vector regression machine and a large database of multiple spacecraft observations. *Journal of Geophysical Research: Space Physics*, 118(5), 2173–2184. <https://doi.org/10.1002/jgra.50226>
- Yermolaev, Y. I., Nikolaeva, N. S., Lodkina, I. G., & Yermolaev, M. Y. (2010). Specific interplanetary conditions for cir-, sheath-, and icme-induced geomagnetic storms obtained by double superposed epoch analysis. *Annales Geophysicae*, 28(12), 2177–2186. <https://doi.org/10.5194/angeo-28-2177-2010>
- Zhang, J., Richardson, I. G., Webb, D. F., Gopalswamy, N., Huttunen, E., Kasper, J. C., et al. (2007). Solar and interplanetary sources of major geomagnetic storms (dst ≤ 100 nt) during 1996–2005. *Journal of Geophysical Research*, 112(A10), A10102. <https://doi.org/10.1029/2007JA012321>
- Zhou, X., & Tsurutani, B. T. (2001). Interplanetary shock triggering of nightside geomagnetic activity: Substorms, pseudobreakups, and quiescent events. *Journal of Geophysical Research*, 106(A9), 18957–18967. <https://doi.org/10.1029/2000JA003028>